Eur. Phys. J. A (2019) **55**: 168
DOI 10.1140/epja/i2019-12858-3

THE EUROPEAN PHYSICAL JOURNAL A

Regular Article – Experimental Physics

Production cross sections of $^{190-193}$Au radioisotopes produced from ^{11}B + ^{nat}W reactions up to 63 MeV projectile energy

Dibyasree Choudhury[1] and Susanta Lahiri[1,2,a]

[1] Saha Institute of Nuclear Physics, 1/AF Bidhannagar, Kolkata-700064, India
[2] Homi Bhaba National Institute, 1/AF Bidhannagar, Kolkata-700064, India

Received: 3 May 2019 / Revised: 11 August 2019
Published online: 30 September 2019

Communicated by S. Bhattacharya

Abstract. This paper reports a new route for production of $^{190-193}$Au radionuclides from a ^{nat}W target. For the first time the production cross section of ^{11}B induced reactions on tungsten for production of $^{190-193}$Au were measured up to 63 MeV projectile energy. High cross section was observed for ^{190,192}Au at the highest energy whereas ^{191,193}Au showed moderate cross section values. The experimentally obtained cross sections were compared with the predictions of the PACE4 and EMPIRE3.2.2 code.

1 Introduction

In recent times, interest towards exploring Auger emitters in medical science has gained momentum. Auger electrons having small range offers cytotoxicity only when incorporated in the cell's DNA or in the immediate vicinity of the nucleus of a cell. The low energy Auger electrons allow targeted therapy at DNA level. ^{198}Au mainly produced from reactors has been vastly explored as a therapeutic radionuclide [1] but on the other hand, the other neutron deficient radionuclides of Au that offer suitable nuclear characteristics such as half-lives, decay modes, high intensity Auger electrons for their clinical applications are much less explored.

Earlier lighter projectiles such as ^{1}H, ^{2}H or ^{4}He particles were used for the production of $^{190-193}$Au radioisotopes. Takács *et al.* [2] produced $^{191-196}$Au radioisotopes from an α-particle irradiated iridium target and studied the excitation function of (α, xn) reaction up to 50 MeV projectile energy. However, production of Au radionuclides from Ir was studied along with several co-produced radioisotopes and the paper mainly focussed on the production of ^{195m}Pt. Bhardwaj *et al.* [3] used the same target-projectile combination to study the cross sections of $^{nat}\mathrm{Ir}(\alpha, \mathrm{xn})^{190-194}$Au reactions up to 55 MeV projectile energy. Ditroi *et al.* [4] produced $^{196m,196g(cum),195g(cum),194,191(cum)}$Au from Au target by $(\mathrm{p}, \mathrm{pxn})$ reaction using proton beam up to 65 MeV. They further compared the experimental results with theoretical codes TALYS1.6 and EMPIRE3.2 code. The Au radioisotopes produced were not in no-carrier-added (NCA) form, thereby limiting their further application. Tarkanyi *et al.* [5] reported the production of $^{191-196,198}$Au from ^{nat}Pt target using ^{1}H beam up to 70 MeV. Maximum cross sections of 530 mb at 42.4 MeV, 673 mb at 36.7 MeV, 454 mb at 22.6 MeV for ^{191}Au, ^{192}Au and ^{193}Au were reported, respectively. In the same year, this group also explored an alternative production route of $^{192-196}$Au by deuteron bombardment on ^{nat}Pt target up to 21 MeV projectile energy [6]. It was found that the cross section was higher for proton induced reactions than deuteron induced ones. But both these papers reported the production of Au along with various other radioisotopes. Indirect production routes of $^{190-193}$Au through spallation reaction on thick cylindrical Pb target by 660 MeV protons (10^{13} protons/s) or as a decay product of Hg isotopes were also reported by Majerle *et al.* [7]. Several radionuclides were also co-produced along with $^{190-193}$Au radionuclides.

For the last two decades our laboratory made a pioneering contribution on developing the neutron-deficient isotope production route by heavy ion activation. A concise literature can be found in ref. [8]. For example, in the context of gold radionuclide production, our laboratory reported production of ^{192,193}Au as daughter product of ^{192,193}Hg which was produced by irradiating tantalum target with 95 MeV ^{16}O beam. However, they did not measure the corresponding excitation function [9]. In the present work, an attempt has been made to systematically measure the production cross section of $^{nat}\mathrm{W}(^{11}\mathrm{B}, \mathrm{xn})$ reaction up to 63 MeV projectile energy and investigate an alternative production route of the $^{190-193}$Au radionuclides. This is the first report on the use of boron beam to produce NCA Au radioisotopes. Interestingly it was found

[a] e-mail: susanta.lahiri@saha.ac.in

Table 1. Irradiation details.

Target[a] (WO_3)	Projectile (^{11}B) energy, MeV			Irradiation time (h)	Integrated charge (μC)
	incident energy	exit energy	energy at the centre of mass		
1	63	62.2	62.6	5.9	296
2	57	56.2	56.6	3.4	337
3	52	51.1	51.5	5.9	296
4	48	47.1	47.6	3.3	152
5	42	41.0	41.5	3.8	123

[a] Target thickness was the same for all, *i.e.* 936 μg/cm^2.

that this production route selectively produced only Au radioisotopes without any radioisotope of other elements.

2 Experimental

2.1 Irradiation parameters

Five WO_3 targets (936 μg/cm^2) were prepared by its deposition on Al foil (7.3 mg/cm^2) via evaporation technique at Tata Institute of Fundamental Research (TIFR) target laboratory. The targets were irradiated one by one with 42–63 MeV ^{11}B beam at BARC-TIFR Pelletron, Mumbai, India. The conventional stack foil technique was not used in this experiment to avoid an excessive energy spread [10]. The exit energy of the projectile was calculated by the software SRIM [11]. The irradiation details are mentioned in table 1. The incident beam was well-collimated on the target holder and the total charge of the incident particle was measured with the help of a Faraday cup placed at the rear end of the target in conjunction with a current integrator (Danfysik). Series of γ-spectra were taken in a p-type HPGe detector of 2.35 keV resolution at 1.33 MeV. The sample to detector distance was $\sim$ 10 cm. The radionuclides were identified from their corresponding photo peaks and decay data. The energy and efficiency calibration of the detector were performed using ^{152}Eu ($T_{1/2}$ = 13.3 a) standard source of known activity (21968 $\pm$ 73 Bq at the day of data acquisition).

2.2 Measurement of experimental cross section

The production cross sections of $^{\text{nat}}$W(^{11}B, xn)$^{190-193}$Au reaction was measured as a function of ^{11}B incident energy by using the following activation equation:

$$A = n\sigma(E)I\left(1 - e^{-\lambda T}\right),$$

where A is the activity (Bq) of a particular radionuclide at EOB, $\sigma(E)$ is the cross section of production of the radionuclide at incident energy E, I is the intensity of boron beam in particles/s, n is the number of atoms/cm^2, λ is the disintegration constant in s^{-1}, T is the duration of irradiation in s.

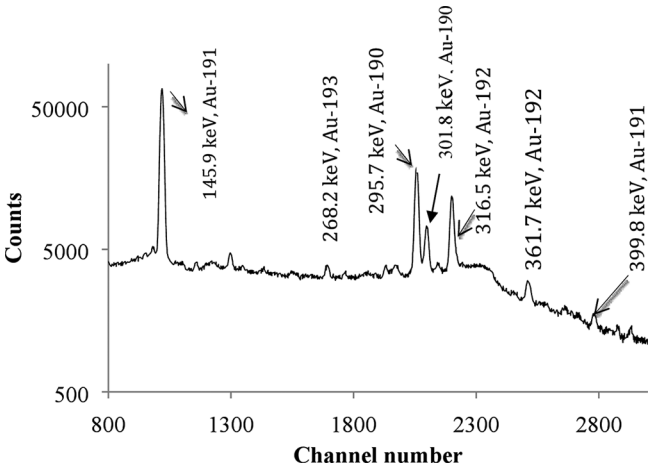

Fig. 1. Gamma spectrum of ^{11}B irradiated $^{\text{nat}}$W target at 63 MeV incident projectile energy, 0.5 h after EOB.

2.3 Error calculation

The uncertainty of each cross section was estimated by considering errors from all sources. The error due to efficiency calibration was insignificant ($\sim$ 0.5%) and has no influence on the total uncertainty. The error due to counting statistics was different for different isotopes at different energies, ^{190}Au (1.42–9.14%), ^{191}Au (6.95–27.4%), ^{192}Au (0.54–11.5%), ^{193}Au (18.31–64.5%). The error in determining the target thickness was $\sim$ 5%. The combined uncertainties due to beam current, incident beam energy, etc., have been estimated as $\sim$ 10%.

2.4 Theoretical cross section calculation

The production cross section of $^{190-193}$Au was compared with theoretical Monte Carlo codes PACE4 [12] and EMPIRE3.2.2 [13]. The evaporation code EMPIRE3.2.2 (version Malta) was designed for simulation of the photons, nucleons, deuterons, tritons, helions, alpha, and light or heavy ions in the low and intermediate energy range. This code employs various nuclear reaction models such as optical model, coupled channels, etc., assuming that all reactions proceed via formation of compound nucleus.

Table 2. Decay characteristics of the produced radionuclides (`https://www.nndc.bnl.gov/chart/chartNuc.jsp`).

Radionuclide	$T_{1/2}$	Decay mode	E_γ, keV, (intensity, %)	E_{Auger}, keV (intensity, %)	Probable production pathways	$E_{\text{Threshold}}$ (MeV)
Au-190	42.8 m	$\varepsilon(100)$	295.7 (71)	7.24 (55.6)	^{182}W(^{11}B, 3n)	32.8
			301.8 (23.4)	51.0 (3.3)	^{183}W(^{11}B, 4n)	39.3
					^{184}W(^{11}B, 5n)	47.2
Au-191	3.18 h	$\varepsilon(100)$	399.8 (4.7%)	7.24 (86)	^{183}W(^{11}B, 3n)	29.8
			421.4 (3.4%)	51.0 (4.4)	^{184}W(^{11}B, 4n)	37.6
Au-192	4.94 h	$\varepsilon(100)$	316.5 (58%)	7.24 (56)	^{184}W(^{11}B, 3n)	30.1
				51.0 (3.4)	^{186}W(^{11}B, 5n)	43.8
Au-193	17.65 h	$\varepsilon(100)$	268.2 (3.6%)	7.24 (78)	^{186}W(^{11}B, 4n)	34.6
				51.0 (4.5)		

Table 3. Yield at EOB of each experimental target and the corresponding Thick Target Yields (TTYs).

Incident projectile energy (MeV)	Yield at EOB							
	^{190}Au		^{191}Au		^{192}Au		^{193}Au	
	experimental target[a], MBq/C	TTY, MBq/C	experimental target, MBq/C	TTY, MBq/C	experimental target, MBq/C	TTY, MBq/C	experimental target, MBq/C	TTY, MBq/C
63	30.7 ± 3.0	200.1	7.8 ± 0.2	99.7	15.8 ± 0.2	107.4	0	27.8
57	16.5 ± 6.5	57.3	8.3 ± 1.5	46.3	7.6 ± 0.05	24.8	2.6 ± 0.5	18.6
52	5.1 ± 0.8	18.1	3.2 ± 0.7	16.9	0.8 ± 0.03	4.8	2.0 ± 0.4	5.29
48	2.5 ± 0.9	3.2	1.97 ± 1.3	6.4	0.6 ± 0.09	1.9	–	–

[a] Each experimental target had the thickness 936 μg/cm^2.

In the EMPIRE code, exciton models with 1.5 mean free path and EGSM (Enhanced Generalized Superfluid Model) level density were used.

The fusion-evaporation code PACE4, a modified version of PACE (projection angular momentum coupled evaporation) was used to calculate the excitation function of residues expected to be produced in ^{11}B-induced reactions on a ^{nat}W target. Fission is considered as a decay mode in this Monte Carlo statistical model code. The finite-range fission barrier of Sierk has been used. A total of 20000 cascades were selected for each simulation. The code internally decides the level densities and masses it needs during de-excitation. The level density parameter was kept $A/10$ (A is the mass number and 10 is a free adjustable parameter) in this calculation.

3 Results and discussion

^{nat}W has five stable isotopes, ^{180}W (0.12%), ^{182}W (26.50%), ^{183}W (14.31%), ^{184}W (30.64%), ^{186}W (28.43%). Therefore, while calculating theoretical production cross sections, a weighted average of each isotope was considered. Time resolved gamma-ray spectroscopy of ^{11}B irradiated $^{nat}WO_3$ target indicated the presence of $^{190-193}$Au radioisotopes (fig. 1). The nuclear characteristics of each of the produced radioisotope have been shown in table 2. Absence of characteristic photopeaks of radioisotope of any other elements makes this production route specific for the Au radioisotopes. The characteristic gamma lines were used in the evaluation of yield at EOB for each investigated radionuclide. The gamma lines which were shared by two Au radionuclides were not included in calculations, even if they had high intensity. For example: the 316.5 keV γ-line has contributions from both ^{192}Au and ^{191}Au, hence it is not taken into consideration. The yields of various gold radionuclides for each experimental target have been provided in table 3.

The thick target yields (TTYs) are the fundamental parameters for practical applications. The individual experimental cross section data sets were fitted with Akima

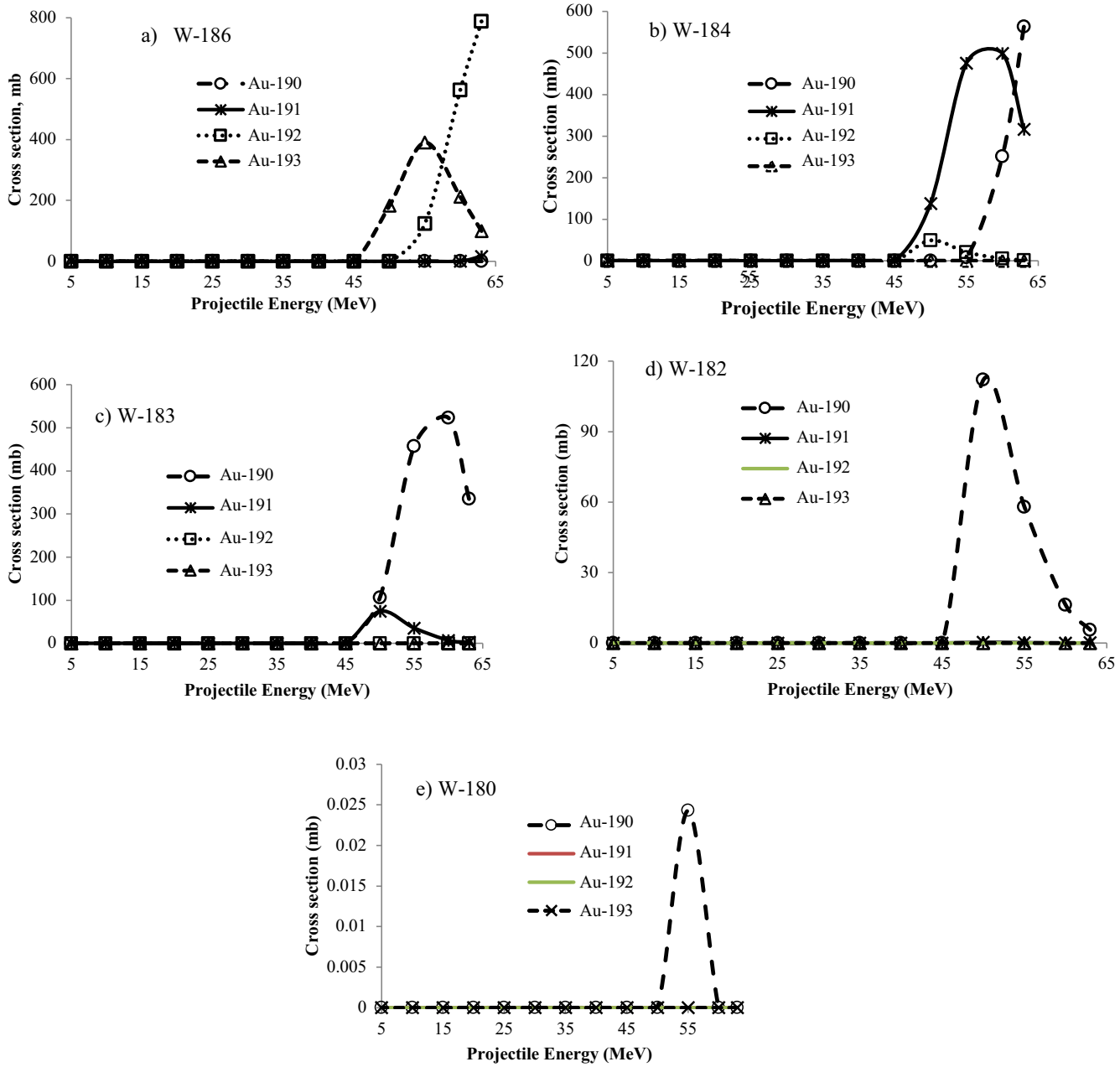

Fig. 2. Production cross sections of $^{190-193}$Au from ^{186}W (a), ^{184}W (b), ^{183}W (c), ^{182}W (d), ^{180}W (e) predicted by the PACE4 code.

Spline fit by Origin Pro software (version 2015) [14] and the integral TTYs were calculated from the threshold up to the incident projectile energies. The stopping power of the beam particles at each energy was calculated with the software SRIM [11]. In table 3 the TTYs at each of the projectile energy have also been provided.

Attempts were made to identify the production pathways mentioned in table 2 responsible for each isotope from PACE4 code. The theoretical cross section of each gold radioisotope from the different stable isotopes of W has been shown in fig. 2(a)–(e). From the plots, it was possible to narrow down the most feasible pathway for each of the products. The following conclusions could be made from the plots:

i) None of the isotopes could be produced from ^{180}W.
ii) Au-191 would be produced from ^{183}W(^{11}B, 3n) or ^{184}W(^{11}B, 4n) reaction while Au-192 would be produced from ^{184}W(^{11}B, 3n) or ^{186}W(^{11}B, 5n) reactions.
iii) The contributing reaction for production of Au-193 is ^{186}W(^{11}B, 4n).

3.1 Cross sections of ^{nat}W(^{11}B, xn) reaction

The measured experimental cross section data is shown in fig. 3(a)–(d), together with the results of theoretical

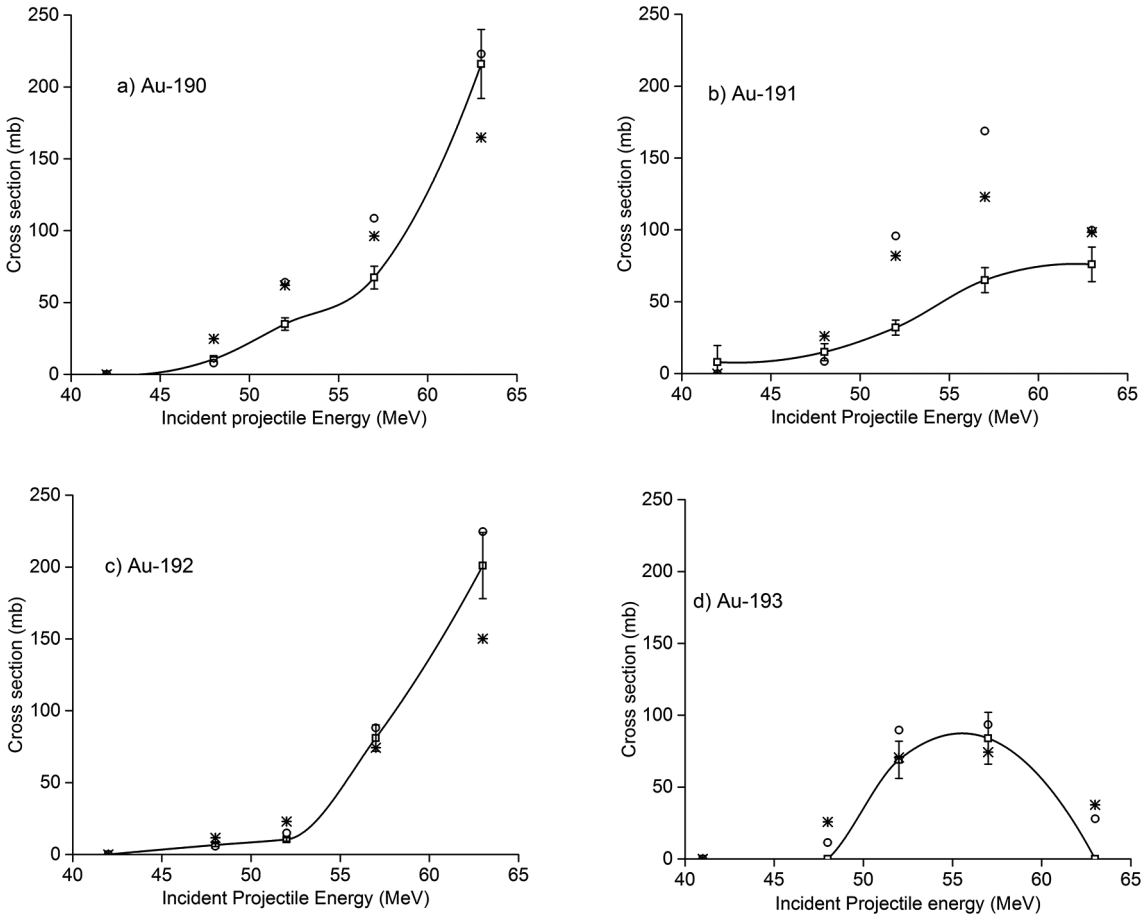

Fig. 3. Excitation function of $^{\mathrm{nat}}\mathrm{W}(^{11}\mathrm{B}, \mathrm{xn})$ reaction from 42–63 MeV.

calculations. The radioisotopes of $^{190-193}$Au may be produced by the $^{\mathrm{nat}}\mathrm{W}(^{11}\mathrm{B}, \mathrm{xn})$ reaction via different reaction channels. The maximum production cross sections for $^{190-193}$Au was different for each isotope. Since the irradiation time for targets 1, 3 and 5 are more than 5 half-lives of ^{190}Au, therefore in the cross section calculation saturation activity and integrated current at 228 min (5 half-lives of ^{190}Au) were considered at the time of cross section calculation.

The cross section of Au-190 increases along with the projectile energy and reaches its maximum at 63 MeV incident energy (216 mb). The experimental cross section is comparable with both PACE and EMPIRE codes except at the highest energy where the EMPIRE value is slightly lower than the experimental value.

The cross section of Au-191 is zero up to 42 MeV but increases after 42 MeV up to 63 MeV with increasing energy. The highest cross section of 76 mb has been observed at 63 MeV. PACE4 and EMPIRE3.2.2 overpredicts the experimental results at 52 and 57 MeV projectile energy.

Au-192 follows a similar trend as Au-190, 191 with the cross section that increases with energy. The highest cross section observed at 63 MeV is 201 mb. The theoretical data reproduce very well the experimental measurements.

In the case of Au-193, the complete excitation plot could be obtained at the experimental energy range studied. The highest cross section of 84 mb has been obtained at 57 MeV. Cross sections predicted by the theoretical codes are matching with the experimental cross section.

In a nutshell, the theoretical cross section and the experimental results matched for all the four radionuclides of Au except few points (*e.g.* 52 and 57 MeV for Au-191). This mismatch might be due to experimental errors.

The cross sections of various gold radionuclides produced by nuclear reactions induced by light ions irradiation have been compared with the present data (table 4). The cross sections related to nuclear reactions induced by heavy ions for Au-191–193 production are of the order 3–5 times less compared to the ones obtained by irradiation with light ions. It is impossible to make a comparison for ^{190}Au production, due to the lack of data for light ions induced reactions.

4 Conclusion

This report offers a feasible production pathway for the no-carrier-added $^{190-193}$Au radioisotopes which are high

Table 4. Comparison of production cross sections reported in the literature with the present experiment.

Reference	Target	Projectile	Au radioisotopes produced	Maximum cross section (projectile energy)
Tarkanyi *et al.* [5]	^{nat}Pt	^{1}H beam up to 70 MeV	^{191}Au	530.4 mb (42.4 MeV)
			^{192}Au	672.6 mb (36.7 MeV)
			^{193}Au	453.9 mb (22.6 MeV)
Ditroi *et al.* [4]	^{nat}Au	^{1}H beam up to 65 MeV	^{191}Au	186.5 mb (63.5 MeV)
Tarkanyi *et al.* [6]	^{nat}Pt	^{2}H beam up to 21 MeV	^{192}Au	9.1 mb (15 MeV)
			^{193}Au	275.5 mb (20.3 MeV)
S. Takács *et al.* [2]	^{nat}Ir	α-beam up to 50.2 MeV	^{191}Au	462 mb (48.52 MeV)
			^{192}Au	763 mb (37.22 MeV)
			^{193}Au	696 mb (45.79 MeV)
Bhardwaj *et al.* [3]	^{nat}Ir	α-beam up to 55 MeV	^{191}Au	800 mb (50 MeV)
			^{192}Au	1000 mb (35 MeV)
			^{193}Au	800 mb (30 MeV)
Present experiment	$^{nat}WO_3$	^{11}B up to 63 MeV	^{190}Au	215 mb (63 MeV)
			^{191}Au	76 mb (63 MeV)
			^{192}Au	201 mb (63 MeV)
			^{193}Au	84 mb (57 MeV)

intensity Auger emitters through $^{nat}W(^{11}B, xn)$ reactions. Though low to moderate production yield has been observed via this route, it is selective for gold radionuclides and no radionuclides of other elements are produced simultaneously, compared to light ion induced production routes. Moreover, one can be even selective to a particular gold radionuclide of interest by choosing enriched target, manipulating the energy window, cooling time, etc. The ^{11}B projectile is easily available in various Tandem Van de Graaff accelerator or pelletron facilities. For example, in India, apart from BARC-TIFR pelletron, the same projectile with the required energy is also available at Inter-University Accelerator Centre (IUAC), New Delhi. There are a number of high current Van de Graaff generators available worldwide. For example, JAEA Tandem accelerator at Tokai-Mura, Japan can also deliver high current ^{11}B. Therefore, such facilities may be exploited to produce Auger electron emitting radionuclides for short range targeted therapy.

Authors gratefully acknowledge the support from TIFR target laboratory and staffs of BARC-TIFR pelletron facility. This work is financially supported by the SINP-DAE 12 five year plan: Trace, Ultratrace Analysis and Isotope Production (TULIP), Government of India.

Data Availability Statement This manuscript has no associated data or the data will not be deposited. [Authors' comment: All data generated during this study are contained in this published article.]

References

1. M. Sadeghi, H. Jabal-Ameli, S.J. Ahmadi, S.S. Sadjadi, M.K. Bakht, J. Radioanal. Nucl. Chem. **293**, 45 (2012).
2. S. Takács, F. Ditroi, Z. Szucs, M. Aikawa, H. Haba, Y. Komori, M. Saito, Appl. Radiat. Isot. **136**, 133 (2018).
3. M.K. Bhardwaj, I.A. Rizvi, A.K. Chaubey, Phys. Rev. C **45**, 2338 (1992).
4. F. Ditroi, F. Tarkanyi, S. Takacs, A. Hermanne, Appl. Radiat. Isot. **113**, 96 (2016).
5. F. Tarkanyi, F. Ditroi, S. Takacs, J. Csikai, A. Hermanne, M.S. Uddin, M. Hagiwara, M. Baba, Y.N. Shubin, A.I. Dityuk, Nucl. Instrum. Methods Phys. Res. B **226**, 473 (2004).
6. F. Tarkanyi, S. Takacs, F. Ditroi, A. Hermanne, Y.N. Shubin, A.I. Dityuk, Nucl. Instrum. Methods Phys. Res. B **226**, 490 (2004).

7. M. Majerle, J. Adam, P. Caloun, S.A. Gustov, V. Henzl, D. Henzlova, V.G. Kalinnikov, M.I. Krivopustov, A. Krasa, F. Krızek, A. Kugler, I.V. Mirokhin, A.A. Solnyshkin, V.M. Tsoupko-Sitnikov, V. Wagner, J. Phys.: Conf. Ser. **41**, 331 (2006).
8. S. Lahiri, J. Radioanal. Nucl. Chem. **307**, 1571 (2016).
9. S. Lahiri, K. Banerjee, N.R. Das, J. Radioanal. Nucl. Chem. **242**, 497 (1999).
10. D. Choudhury, N. Naskar, S. Lahiri, Radiochim. Acta **106**, 743 (2018).
11. J.F. Zeigler, J.P. Bierserk, U. Littmark, *The Stopping and Ranges in Solids* (Pergamon Press, New York, 1985).
12. O.B. Tarasov, D. Bazin, Nucl. Instrum. Methods B **204**, 174 (2003).
13. M. Herman, R. Capote, B.V. Carlson, P. Oblozinsky, M. Sin, A. Trkov, H. Wienke, V. Zerkin, Nucl. Data Sheets. **108**, 2655 (2007).
14. `http://OriginLab.com/2015`.